RAA 2015 Vol. **15** No. **7**, 1068–1076 doi: 10.1088/1674–4527/15/7/014
http://www.raa-journal.org *http://www.iop.org/journals/raa*

***R**esearch in*
***A**stronomy and*
***A**strophysics*

Photometric Calibration of the Lunar-based Ultraviolet Telescope for Its First Six Months of Operation on the Lunar Surface *

Jing Wang[1,2], Li Cao[1,2], Xian-Min Meng[1,2], Hong-Bo Cai[1,2], Jing-Song Deng[1,2], Xu-Hui Han[1,2], Yu-Lei Qiu[1,2], Fang Wang[1,3], Shen Wang[1,2], Wei-Bin Wen[1,3], Chao Wu[1,2], Jian-Yan Wei[1,2] and Jing-Yao Hu[1]

[1] National Astronomical Observatories, Chinese Academy of Sciences, Beijing 100012, China
[2] Key Laboratory of Space Astronomy and Technology, National Astronomical Observatories, Chinese Academy of Sciences, Beijing 100012, China; *wj@nao.cas.cn*
[3] Key Laboratory of Lunar and Deep Space Exploration, National Astronomical Observatories, Chinese Academy of Sciences, Beijing 100012, China

Received 2014 August 25; accepted 2014 December 11

Abstract We describe the photometric calibration of the Lunar-based Ultraviolet Telescope (LUT), the first robotic astronomical telescope working on the lunar surface, for its first six months of operation on the lunar surface. Two spectral datasets (set A and B) from near-ultraviolet (NUV) to the optical band were constructed with 44 International Ultraviolet Explorer (IUE) standards, because of the LUT's relatively wide wavelength coverage. Set A was obtained by extrapolating the IUE NUV spectra ($\lambda < 3200$ Å) to the optical band based upon the theoretical spectra of stellar atmosphere models. Set B was composed of theoretical spectra from 2000 Å to 8000 Å extracted from the same model grid. In total, seven standards have been observed in 15 observational runs until May 2014. The calibration results show that the photometric performance of LUT is highly stable in its first six months of operation. The magnitude zero points obtained from the two spectral datasets are also consistent with each other, i.e., $\mathrm{zp} = 17.54 \pm 0.09$ mag (set A) and $\mathrm{zp} = 17.52 \pm 0.07$ mag (set B).

Key words: space vehicles: instruments — telescopes — techniques: photometric — ultraviolet: general

1 INTRODUCTION

The Lunar-based Ultraviolet Telescope (LUT) on board the first Chinese lunar lander (Chang'e-3) is the first robotic astronomical telescope to operate on the lunar surface in the history of lunar exploration. It was developed by National Astronomical Observatories, Chinese Academy of Sciences and the Xi'an Institute of Optics and Precision Mechanics, Chinese Academy of Sciences. Taking advantage of both the very slow rotation and extremely tenuous atmosphere of the Moon, the main scientific goals of LUT are (1) to continuously monitor bright variable stars in the near-ultraviolet

* Supported by the National Natural Science Foundation of China.

(NUV) band for as long as a dozen days; and (2) to perform a dedicated sky survey at low Galactic latitude in the NUV band. The survey can cover regions that were avoided by the Galaxy Evolution Explorer (GALEX) mission (Martin et al. 2005). We refer the readers to Cao et al. (2011) for a detailed description of the scientific goals and mission design of LUT, and to Wang et al. (2011) for a discussion on the potential effect of the lunar exosphere on the NUV sky background emission detected by LUT.

LUT was successfully launched on 2013 December 2 by a Long March 3B rocket, and had its first light on 2013 December 16, two days after Chang'e-3 landed on the lunar surface. By May 2014, LUT had smoothly operated on the Moon for six months, and acquired a total of more than 50 000 images. This paper describes the photometric calibration for its first **six** months of operation on the lunar surface.

Section 2 presents an overview of the instrument. The calibration in laboratory at pre-launch is given in Section 3. Section 4 describes the calibration procedures, including spectral datasets construction, observations, data reductions, and the final calibration results. A summary is provided in Section 5.

2 INSTRUMENT OVERVIEW

A cross section of LUT is shown in Figure 1. The telescope is an F/3.75 Ritchey-Chrétien system with an aperture of 150 mm. A fixed flat mirror (the third mirror) is used to reflect light to the Nasmyth focus to reduce the length of the whole instrument. A two-lens field corrector is located in front of the focal plane, and is used to correct the field curvature. A coating that improves NUV transmission is applied on the last lens. The transparency of the coating peaks at 2500 Å, and has an effective width of 1080 Å. A UV-enhanced 1024×1024 AIMO CCD E2V47–20 (manufactured by the e2v company), operated in frame transfer mode, is chosen as the detector mounted at the Nasmyth focus. The CCD has a pixel size of 13 μm and can be thermoelectrically cooled by as much as 40°C below its ambient temperature. A rotatable flat mirror (the pointing flat mirror) with a size of 200 mm×166 mm is mounted on a two-dimensional gimbal, which is used to point toward and track a given celestial object. The gimbal has a designed pointing accuracy of 0.05°, which corresponds to about 38 pixels on the focal plane. Two LED lamps with a center wavelength of 286 nm are equipped to provide an internal flat field. The field-of-view of LUT is $1.36\times1.36\ \mathrm{degree}^2$, which corresponds to a pixel scale of $4.76''\ \mathrm{pixel}^{-1}$.

The main characteristics of LUT are summarized in Table 1. A system flow chart illustrating how the LUT functions was presented as figure 1 in Cao et al. (2011).

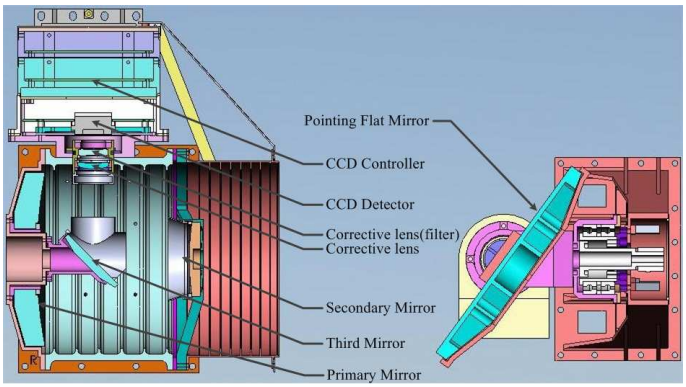

Fig. 1 A cross sectional view of LUT. The main components are labeled.

Table 1 The Main Characteristics of LUT

Item (1)	Value (2)
Telescope:	
Type	Ritchey-Chrétien
Primary diameter	150 mm
Focal length	563 mm
Field of View	1.36×1.36 degree^2
Peak efficiency	0.08 at 2500 Å
Band width (FWHM)	1080 Å
Pointing:	
Pointing flat mirror	200 mm $\times$ 166 mm
Gimbal	2-dimensions
Gimbal accuracy	0.05°
Detector:	
Type	UV enhanced frame transfer AIMO CCD47-20
Active pixels	1024×1024
Pixel size	13 μm
Pixel scale	$4.76'' \text{ pixel}^{-1}$

3 THROUGHPUT DETERMINATION AT PRE-LAUNCH

The throughput of LUT at different wavelengths was measured before launch in a laboratory by a dedicated calibration system. The calibration system was composed of a deuterium lamp (type L1314 by Hamamatsu, Inc.), a halogen-tungsten lamp (type L10296 by Hamamatsu, Inc.), a monochromator (type 207D by McPherson, Inc.), an adjustable diaphragm and two pre-calibrated sensors. During the test, collimated monochromatic light produced by the monochromator was directed into the telescope without any intervening optical elements in the light path.

Figure 2 presents the normalized throughput curve of LUT as a function of wavelength. The throughput peaks at around 2500 Å with a peak value of $\approx 8\%$. The effective wavelength and width have been calculated under different definitions. The effective wavelength defined as the wavelength-weighted average is calculated to be 3046 Å. The effective wavelength defined by Schneider et al. (1983)

$$\ln \lambda_{\rm eff} = \frac{\int d(\ln \lambda) S_\lambda \ln \lambda}{Q} \tag{1}$$

is calculated to be 2941 Å, where $Q = \int S_\lambda d \ln \lambda = 0.027$ is a flux sensitive quantity and S_λ the optical efficiency at wavelength λ. The full width at half maximum (FWHM) of the curve is determined to be about 1080 Å. The rms fractional width σ of the throughput, defined as

$$\sigma^2 = \frac{\int S_\lambda \ln^2(\frac{\lambda}{\lambda_{\rm eff}}) d \ln \lambda}{Q} \tag{2}$$

is calculated to be 0.146.

4 PHOTOMETRY CALIBRATION

4.1 Magnitude System

The AB magnitude system is adopted for LUT observations. This photometry system was first defined by Oke & Gunn (1983), and has been widely used since its application in the Sloan Digital Sky Survey (Fukugita et al. 1996). It has also been used by the GALEX mission (Morrissey et al. 2005).

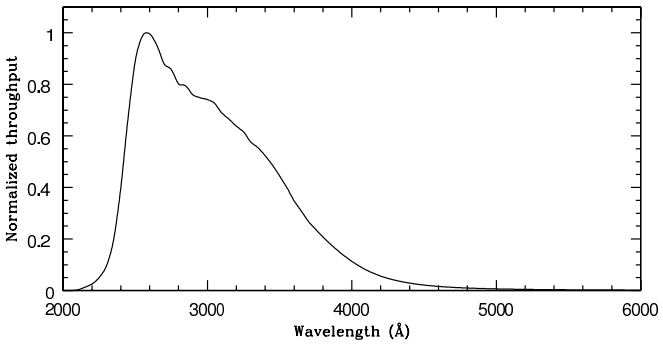

Fig. 2 The normalized throughput of LUT as a function of wavelength.

The broadband AB magnitude of an object detected by LUT is defined as

$$m_{\rm AB} = -2.5 \log \frac{\int f_\nu S_\nu d \ln \nu}{\int S_\nu d \ln \nu} - 48.6, \tag{3}$$

where f_ν is the specific flux density of the object in the unit of $\rm erg\,s^{-1}\,cm^{-2}\,Hz^{-1}$, and S_ν the LUT's total throughput at frequency ν. The throughput S_ν measured in the laboratory includes contributions from the optical efficiency of the telescope and pointing flat mirror, the transparency of the NUV coating, and the quantum efficiency of the detector.

The actual brightness $m_{\rm LUT}$ of an object observed by LUT is transformed from the observed instrumental magnitude $m_{\rm inst}$ through $m_{\rm LUT} = m_{\rm inst} + {\rm zp}$, where zp is the zero point of the LUT magnitude system that should be determined by observing standard stars. Having the throughput S_ν measured, one can convert the observed magnitude to its physical flux for a given object with known spectral shape. In the conversion, there is no free parameter in the integrand of Equation (3), except for a constant multiplier.

4.2 Photometric Standard Stars

The photometric calibration of LUT is based on the UV spectral atlas of standard stars (Wu et al. 1998) provided by the International Ultraviolet Explorer (IUE) mission[1]. This atlas was used because these stars (1) are bright enough for LUT to observe, (2) have reliable absolute specific flux in NUV, after the exclusion of stars with known variability and peculiarity, (3) have known spectral types and luminosity classes (as well as parameters characterizing their stellar atmosphere), (4) have comprehensive coverage on the H-R diagram, and (5) are nearly uniformly distributed on the sky. The NUV spectra of all the IUE standard stars were taken in the low dispersion mode (LWP/R, 1850-3300 Å) with a spectral resolution of ~ 6 Å. Their specific fluxes are uniformly obtained from the NEWSIPS pipeline, which involves the best treatment of noise and the latest instrument parameters (Nichols & Linsky 1996). The calibration of the IUE satellite was based on the stellar atmosphere model of white dwarf G 191B2B (Nichols & Linsky 1996), which is the same method used for calibrating the Hubble Space Telescope (HST) Faint Object Spectrograph. Although the uncertainty in the atmosphere model of G 191B2B is only $\sim$2%, the calibrated flux of IUE is systematically lower than that of HST by $\sim$6%. This is because the model's effective temperature adopted by IUE is lower than that adopted by HST (58 000 vs. 63 000 K).

There are a total of 44 IUE standards located in the sky region available to LUT, as shown in Figure 3. The total available sky area is about 3600 degree^2, which results in a surface density

[1] The IUE standard library can be found in the website *http://www-int.stsci.edu/∼jinger/iue.html*. There are a total of 476 standard stars.

Table 2 IUE standards observed by LUT until May 2014

Star	s.p. type	α (J2000)	δ (J2000)	m_v (mag)	$E(B-V)$ (mag)	$T_{\rm eff}$ (K)	$\log g$	Fe/H	$m_{\rm ck04}$ (mag)	$m_{\rm iue}$ (mag)	Reference
(1)	(2)	(3)	(4)	(5)	(6)	(7)	(8)	(9)	(10)	(11)	(12)
HD 131873	K4III	14 50 42.3	+74 09 20	2.07	0.04	4077	1.7	–0.10	6.52	6.52	Koleva & Vazdekis (2012)
HD 153751	G5III	16 45 58.2	+82 02 14	4.23	0.00	5150	2.54	0.00	7.35	7.36	Soubiran et al. (2010)
HD 159181	G2Ib-IIa	17 30 26.0	+52 18 05	2.80	0.09	5325	1.51	–0.02	6.09	6.08	Koleva & Vazdekis (2012)
HD 164058	K5III	17 56 36.4	+51 29 20	2.23	0.01	3990	1.64	0.11	6.87	6.86	Prugniel et al. (2011)
HD 185395	F4V	19 36 26.5	+50 13 16	4.48	0.00	6700	4.30	0.01	6.34	6.41	Cunha et al. (2000)
HD188665	B5V	19 53 17.4	+57 31 25	5.14	0.02	14893	3.86	–0.17	5.26	5.33	Fitzpatrick & Massa (2005)
HD 214470	F3III-IV	22 35 46.1	+73 38 35	5.08	0.00	6637	3.59	0.09	7.18	7.22	Soubiran et al. (2010)

of $\sim 0.01\ \mathrm{degree}^{-2}$ for the 44 standards. Due to the available range of the gimbal rotation, LUT can only access a small sky area of $\sim 400\ \mathrm{degree}^2$ at a given time, which means on average four standards are observable by LUT at a given time. Such a surface density and the uniform distribution ensure that a photometric calibration can be done at any epoch and that the evolution of the LUT's efficiency can be continuously monitored. In addition, the model dependence of the final calibration results can be alleviated by applying statistical analysis to multiple standards (see Sect. 4.5 below).

For the purpose of photometric calibration, two spectral datasets of the 44 IUE standards were constructed to cover the wide wavelength range of the LUT throughput (Fig. 2). The spectral atlas provided by the IUE mission has a red cutoff at 3200 Å, which would result in an underestimate of the expected brightness if the original atlas was used in Equation (3). The level of underestimation is expected to be more significant for red stars than for blue stars, simply because the peak of the SED of a star shifts toward a longer wavelength when the stellar surface temperature decreases. The ATLAS9 model atmospheres (Castelli & Kurucz 2003) were adopted to solve this problem. With the theoretical spectra extracted from the model grid, we constructed two spectral datasets (set A and B) for the 44 IUE standards. Set A was obtained by combining the IUE observed NUV spectra ($\lambda < 3200$ Å) with the theoretical spectra beyond 3200 Å. Set B was composed of theoretical spectra from 2000 Å to 8000 Å. We will show below that these two datasets return consistent calibration results within their uncertainties.

The theoretical spectra that we practically used were acquired as follows. At first, a model spectrum was extracted from the original ATLAS9 grid by a 3-dimensional linear interpolation for each of the 44 IUE standards. The three physical parameters used in the interpolation are the measured effective temperature, surface gravity and metal abundance that are collected from recent literature (see Table 2). Secondly, each extracted model spectrum was reddened by its color excess $E(B-V)$ value through the IRAF.synphot.calcspec[2] task to account for the expected Galactic extinction. The $E(B-V)$ value was taken from the IUE standard catalog, and the extinction curve from Calzetti et al. (1994). Finally, the absolute flux level of each reddened model spectrum was determined from the V-band magnitude reported in SIMBAD.

Figure 4 shows the spectra constructed in this way (2000 Å to 8000 Å, both set A and B) of a standard star HD 188665 (spectral type B5V) as an example. After construction of the theoretical spectrum, two expected magnitudes (set A and B) in the LUT system were subsequently calculated through Equation (3) for each of the standards.

4.3 Observations of the Standards

Seven standards have been observed until May 2014 in 15 observational runs. The details of the seven standards are listed in Table 2. The effective temperature, surface gravity and abundance collected

[2] IRAF is distributed by the National Optical Astronomy Observatory, which is operated by the Association of Universities for Research in Astronomy, Inc., under cooperative agreement with the National Science Foundation.

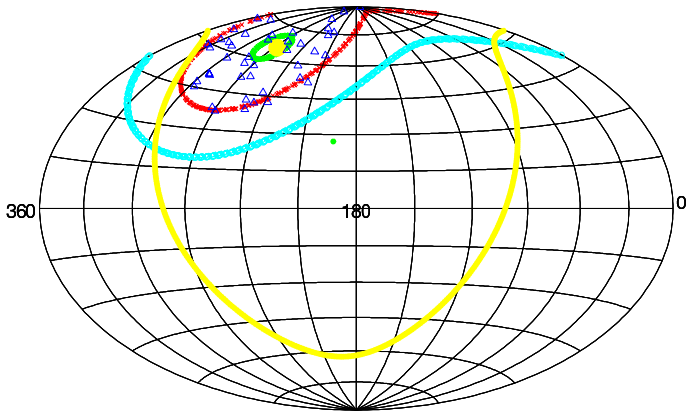

Fig. 3 The available sky of LUT and the distribution of the 44 IUE standards in the J2000 mean equatorial coordinate system. The LUT's available sky is located between the red and green circles. The locus of the zenith of LUT is shown by the cyan curve. The Galactic plane and north Galactic pole are shown by the yellow curve and small green dot, respectively. The large yellow point marks the north pole of the Moon. The distribution of the IUE standards is shown by the open blue triangles.

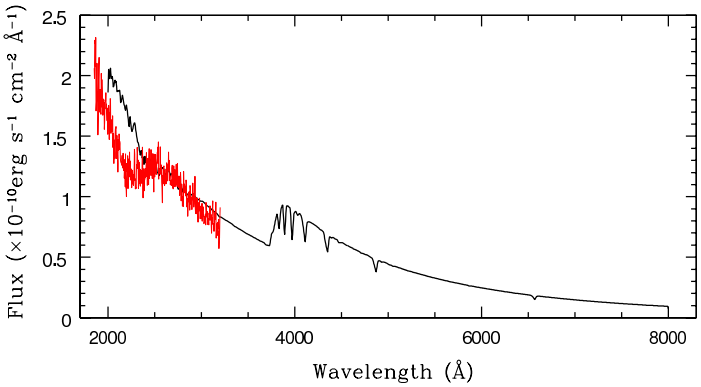

Fig. 4 The spectra of a standard star HD 188665 in the unit of flam. The black curve shows the spectrum extracted from the ATLAS9 stellar atmosphere model, and the red curve the NUV spectrum observed by IUE. The absolute flux level of the model spectrum is determined by its V-band brightness.

from the literature are tabulated in Columns (7), (8) and (9), respectively. Columns (10) and (11) list the expected magnitudes for set B and A, respectively. An appropriate observational strategy was designed to remove the strong stray light caused by sunshine. The telescope pointing was fixed with respect to the Moon in each observational run, which is required to be long enough, i.e., close to 30 minutes, to allow the star to have a significant shift with respect to the fixed stray light pattern. Each run is composed of a series of short exposures with duration of 2 to 10 seconds depending on the brightness of the standards. Thanks to the slow rotation of the Moon, the shift of a star on the focal plane within each exposure is negligible compared with the size of the point-spread-function (PSF).

4.4 Data Reductions

Reductions of the raw calibration data were performed with the general LUT reduction pipeline. The pipeline is described in detail in a companion paper (Meng et al. in preparation). A brief summary of the pipeline is given below. At first, an overscan correction was applied to all the images taken by LUT. The overscan-corrected images in each observational run were then grouped according to the pointing of the gimbal with respect to the Moon. The total time elapsed in each group is required to be less than 30 minutes to avoid a significant evolution of both the level and pattern of the underlying stray light. For each group, the component of stray light in a given image was acquired by combining all the images (except the given one) in the group without any image shift, in which a median value was extracted for each pixel. Before the combination, the images that should be combined were scaled in advance to have a common background level which was determined by image statistics on the whole CCD of the given image. The underlying stray light was then removed from the given image by the constructed stray light image. We emphasize that both the underlying bias and dark current were simultaneously removed along with the stray light in this procedure. Each of the images that had stray light removed was subsequently normalized by a composite flat field. In addition to the internal flat field provided by the LED lamps that can only correct nonuniformity in CCD quantum efficiency on the pixel scale, a super flat field was acquired by a drift observation of a normal star. As an example, Figures 5 and 6 show a flat field that was finally used and a reduced image for HD 188665, respectively.

The instrumental magnitude of each observed standard star was obtained by aperture photometry through the IRAF/apphot task. The aperture with a fixed radius of 7 FWHM was used in our photometry to ensure that almost all the signal from the star was enclosed in the aperture. The FWHM of each frame was determined by fitting the PSF by a Moffat profile. The background level around the object was measured from an annulus with a width of 5 pixels out of the photometric aperture.

4.5 Magnitude Zero Point

The measured instrumental magnitudes with an arbitrary magnitude zero point of $\mathrm{zp}' = 25$ mag are listed in Column (2) of Table 3. The 1σ errors reported in the column were derived from the statistics on the multiple observations in each observational run. Each error contains the contributions mainly

Table 3 A Comparison between the Measured Instrumental Magnitudes and the Expected Ones

Star	m_{inst} (mag)	$\mathrm{zp}' - \mathrm{zp}$ (mag)	Epoch
(1)	(2)	(3)	(4)
HD 131873	14.16 ± 0.03	7.64	2014/05/19
HD 153751	14.75 ± 0.02	7.40	2014/05/19
HD 159181	13.51 ± 0.01	7.41	2014/01/12
	13.52 ± 0.02	7.43	2014/01/16
	13.55 ± 0.01	7.45	2014/02/10
HD 164058	14.40 ± 0.02	7.53	2014/01/12
	14.44 ± 0.30	7.57	2014/02/10
	14.37 ± 0.01	7.50	2014/02/15
	14.42 ± 0.03	7.54	2014/03/16
HD 185395	13.79 ± 0.01	7.45	2013/12/23
	13.79 ± 0.01	7.46	2014/02/15
	13.82 ± 0.01	7.48	2014/02/18
	13.78 ± 0.02	7.45	2014/03/16
HD 188665	12.71 ± 0.01	7.45	2013/12/23
HD 214470	14.61 ± 0.02	7.44	2014/05/19

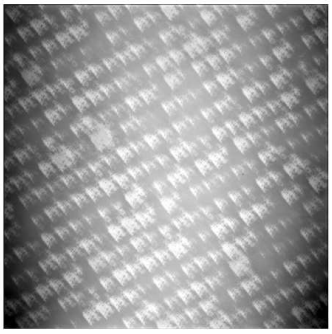

Fig. 5 A flat field that was finally used derived from a combination of the internal flat field provided by the LED lamps and a super flat field.

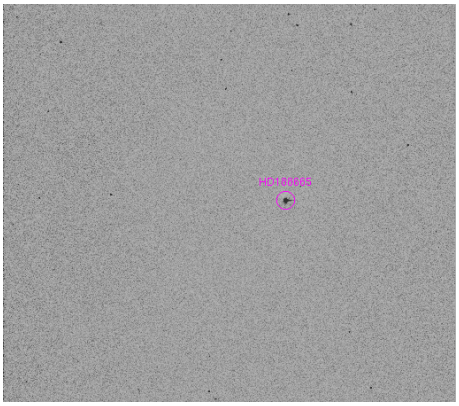

Fig. 6 A reduced image for standard star HD 188665.

from the photon fluctuation, stray light removal and image normalization. Because of their high signal-to-noise ratios, the uncertainty due to the photon fluctuation is generally as low as 0.001–0.003 magnitudes for all the observed standards, which is much smaller than the reported errors. Our experiments show that a large fraction of the errors comes from the insufficient image normalization. As described in Section 4.4, the flat field that we finally used is a combination of the intrinsic flat field and the super flat field. The intrinsic flat field can only correct the nonuniformity in CCD quantum efficiency on the scale of pixels, but the super flat field compensates the nonuniformity on a larger scale of hundreds of pixels. Nonuniformity on a medium scale of tens of pixels can therefore not be perfectly corrected by the combined flat field.

Column (3) in Table 3 lists the reduced zero points $\mathrm{zp}' - \mathrm{zp}$ based on the expected magnitudes calculated from the spectral dataset constructed from set B (i.e., Column (10) in Table 2). One can see from the table that three standards have been observed for three to four runs in the LUT's first six months of operation. The resulting magnitude zero points of these three standards show non-detectable variation (within their uncertainties) with time, which indicates a highly stable performance of LUT during its first six months of operation.

A statistic on all the calibration results from different standards at different times yields two consistent average magnitude zero points obtained from the two constructed spectral datasets, i.e., $\mathrm{zp} = 17.54 \pm 0.09$ mag (set A) and $\mathrm{zp} = 17.52 \pm 0.07$ mag (set B). Both reported errors correspond

to a 1σ significance level. These reported errors are clearly larger than the errors inferred from a single standard. The increase in error can be easily understood because the expected magnitude of a standard depends on many factors, including the IUE spectral/ATLAS9 model calibration (see Sect. 4.2 for the details), the V-band magnitude, the level of extinction and the parameters used to define the atmosphere model.

5 SUMMARY

We have described the photometric calibration of LUT for its first **six** months of operation on the lunar surface. Two spectral datasets from NUV to the optical band were constructed for photometric calibration with 44 IUE standards, because of the relatively wide wavelength coverage of LUT. The calibration results indicate that the photometric performance of LUT has been highly stable during its first six months of operation. The magnitude zero points inferred from the two spectral datasets are highly consistent with each other.

Acknowledgements The authors thank the outstanding work of the LUT team and support by the team from the ground system of the Chang'e-3 mission. This study is supported by the Key Research Program of Chinese Academy of Sciences (KGED-EW-603) and by the National Basic Research Program of China (973 program, Grant No. 2014CB845800). JW is supported by the National Natural Science Foundation of China under Grant 11473036. MXM is supported by the National Natural Science Foundation of China under Grant 11203033.

References

Calzetti, D., Kinney, A. L., & Storchi-Bergmann, T. 1994, ApJ, 429, 582
Cao, L., Ruan, P., Cai, H., et al. 2011, Science China Physics, Mechanics, and Astronomy, 54, 558
Castelli, F., & Kurucz, R. L. 2003, in IAU Symposium, 210, Modelling of Stellar Atmospheres, ed. N. Piskunov, W. W. Weiss, & D. F. Gray, 20P
Cunha, K., Smith, V. V., Boesgaard, A. M., & Lambert, D. L. 2000, ApJ, 530, 939
Fitzpatrick, E. L., & Massa, D. 2005, AJ, 129, 1642
Fukugita, M., Ichikawa, T., Gunn, J. E., et al. 1996, AJ, 111, 1748
Koleva, M., & Vazdekis, A. 2012, A&A, 538, A143
Martin, D. C., Fanson, J., Schiminovich, D., et al. 2005, ApJ, 619, L1
Morrissey, P., Schiminovich, D., Barlow, T. A., et al. 2005, ApJ, 619, L7
Nichols, J. S., & Linsky, J. L. 1996, AJ, 111, 517
Oke, J. B., & Gunn, J. E. 1983, ApJ, 266, 713
Prugniel, P., Vauglin, I., & Koleva, M. 2011, A&A, 531, A165
Schneider, D. P., Gunn, J. E., & Hoessel, J. G. 1983, ApJ, 264, 337
Soubiran, C., Le Campion, J.-F., Cayrel de Strobel, G., & Caillo, A. 2010, A&A, 515, A111
Wang, J., Deng, J. S., Cui, J., et al. 2011, Advances in Space Research, 48, 1927
Wu, C., Mo, J., Crenshaw, D. M., & Schiffer, F. H. 1998, in ESA Special Publication, 413, Ultraviolet Astrophysics Beyond the IUE Final Archive, ed. W. Wamsteker, R. Gonzalez Riestra, & B. Harris, 751